Large Deformation Finite Element Analysis for Offshore Applications

Article · January 2008

CITATIONS
23

READS
1,442

5 authors, including:

Mark Randolph
University of Western Australia
349 PUBLICATIONS **9,206** CITATIONS
SEE PROFILE

Dong Wang
Ocean University of China
77 PUBLICATIONS **927** CITATIONS
SEE PROFILE

Hongjie Zhou
Norwegian Geotechnical Institute
17 PUBLICATIONS **424** CITATIONS
SEE PROFILE

M.s. Hossain
Dhaka University of Engineering & Technology
31 PUBLICATIONS **398** CITATIONS
SEE PROFILE

The 12th International Conference of
International Association for Computer Methods and Advances in Geomechanics (IACMAG)
1-6 October, 2008
Goa, India

Large Deformation Finite Element Analysis for Offshore Applications

M.F. Randolph, D. Wang, H. Zhou and M.S. Hossain
Centre for Offshore Foundation Systems, University of Western Australia, Perth, Australia

Y. Hu
Department of Civil Engineering, Curtin University of Technology, Perth, Australia

Keywords: clay, finite element analysis, large deformation, deep penetration

ABSTRACT: Many applications in offshore engineering involve large movements of foundation or anchoring elements relative to the seabed. These include penetration of foundations for mobile drilling platforms, partial embedment and lateral motion of pipelines, interpretation of penetrometer tests and pullout of anchors. Numerical analysis requires techniques that allow simulation of large strains and deformations within the soil, with the ability to track changes in originally horizontal strength contours, and also changes in strength due to cumulative shear strain and hence gradual remoulding. The paper gives an overview of a simple but powerful tool for large deformation finite element analysis, where small strain Lagrangian analysis steps are interleaved with Eulerian updating of the mesh and interpolation of all field quantities. The technique is illustrated with four applications, in each of which new insight is demonstrated through the ability to accommodate large changes in geometry of the problem and also in the soil properties. It is demonstrated that the very simple approach followed appears to give robust and accurate results. Comparisons are included between results based on locally developed finite element and mesh generation software and commercial packages such as ABAQUS.

1 Introduction

Geotechnical applications in offshore engineering often involve large displacements of structural elements, such as a foundation or pipeline, relative to the seabed sediments. Quantification of soil-structure interaction must therefore consider geometric non-linearity due to changes in the surface profile, or distortion of initially horizontal soil layers, in addition to the material non-linearity that is an intrinsic aspect of soil behaviour. Over the last decade, a simple practical approach to large deformation analysis, based on the initial work of Hu and Randolph (1998a), has been applied to a variety of offshore design problems. The aim of this paper is firstly to summarise the approach in relation to more sophisticated ALE techniques, and secondly to illustrate key aspects of the approach in relation to four problems involving pipelines and foundations penetrating from the soil surface, deep penetration allowing for softening of the soil, and breakout of pre-embedded circular and square anchors.

The early development of large deformation finite element (LDFE) analysis focused on an updated Lagrangian approach, where the finite element mesh was tied to the solid and sophisticated stress and strain formulations were required to deal with the large cumulative strains and rotations in each element (Bathe et al., 1975; Hughes and Winget, 1980). The updated Lagrangian approach eventually becomes limited by the gross distortion of elements as the analysis progresses. This difficulty was overcome by the so-called arbitrary Largangian-Eulerian (ALE) modification, where Eulerian flow of the solid through the mesh was included (Liu et al., 1986; Ghosh and Kikuchi, 1991; Liu et al, 1998; van Haaren et al., 2000). Specific application of the ALE approach to geomechanics problems has been considered recently by Nazem et al. (2006).

The developments cited above have tended to follow a formal approach, with large strain formulations for the Lagrangian steps and in many cases incorporating ‘convection’ of the solid relative to the finite element mesh implicitly in the finite element equations. The large strain formulations become increasingly difficult to implement for more complex soil constitutive models. By contrast, the approach proposed by Hu and Randolph (1998a), referred to as Remeshing and Interpolation Technique with Small Strain (RITSS), is simpler, based on standard small strain Lagrangian increments but with periodic remeshing followed by interpolation of all stresses and material properties. The latter may include user-defined history variables such as the original depth of that ‘particle’ of soil, or cumulative plastic shear strain (for calculating damage). The principle is that each new remeshing stage constitutes a new problem, albeit with boundary geometries and internal stresses that reflect the preceding sequence of increments. The advantage of the approach is that the remeshing and interpolation algorithms may be coupled with any standard finite element package through user-written interface codes. The

robustness of the approach has been demonstrated by, for example, comparison of the penetration resistance of cylindrical or spherical penetrometers with plasticity solutions (Lu et al., 2000; Zhou and Randolph, 2007).

Much of the early application of LDFE in geomechanics was built around the finite element code, AFENA (Carter and Balaam, 1995), and addressed problems including deep penetration of skirted foundations (Hu et al., 1999) and punch through of foundations on layered soils (Wang and Carter, 2002). More recently, the technique has been coupled with commercial codes such as ABAQUS (Wang et al., 2007; Liyanapathirana, 2008) and LS-DYNA (Konuk and Yu, 2007). The examples presented later include comparative analyses based on AFENA and ABAQUS, and attempt to illustrate the versatility of the approach. The problems addressed (see Figure 1) range from the large geometric changes associated with near-surface penetration or breakout of anchors, to analysis of steady-state deep penetration in rate-dependent, strain-softening soil.

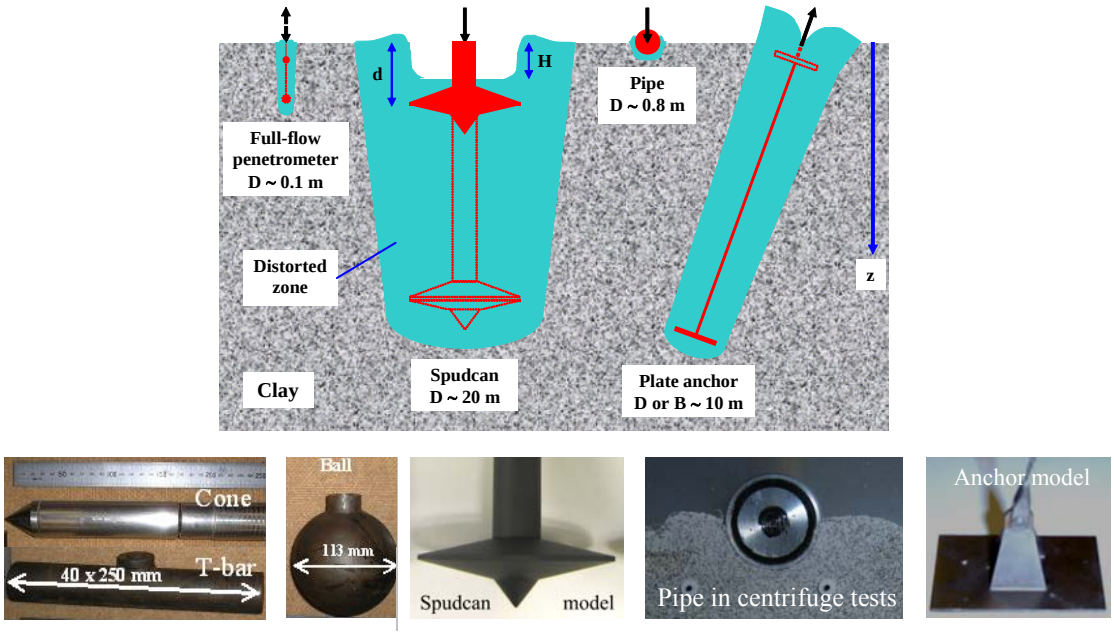

Figure 1. Example problems addressed

2 Methodology

The overall scheme of the RITSS approach is demonstrated in Figure 2a, consisting of a series of small-strain analysis increments, followed by remeshing, and then interpolation of the field quantities (stresses and material properties) on the Gauss points from the old mesh to the new mesh (Hu and Randolph, 1998a). The sequence of small-strain increments, remeshing and interpolation can be repeated until the required displacement has been reached. Figure 2b details the procedure for RITSS coupled with ABAQUS/Standard, where ABAQUS is called by a master program (written in Fortran language) to conduct mesh generation and small strain calculations in each incremental step. Several Python (the build-in script language of ABAQUS) files were coded beforehand in order to extract necessary data from result files and control the mesh density during mesh regeneration (Wang et al., 2006). The recovery and interpolation of stresses and material parameters are carried out externally by subroutines written in Fortran. Both AFENA and ABAQUS based large deformation analyses are performed continuously and automatically without requiring any intervention from the user. The ABAQUS based RITSS, however, is more versatile than using AFENA, as ABAQUS includes powerful algorithms for mesh generation and computational efficiency, which is especially important for simulating three-dimensional (3D) problems. For the 3D simulations, limited by the state-of-the-art of meshing technique, quadratic tetrahedral elements rather than octahedron elements are used to mesh irregular 3D geometries.

During mesh regeneration, an *h*-adaptive technique may be applied in an attempt to produce an optimal mesh at each stage. However, in some cases this leads to unpredictable evolution of the mesh during continuous deformation, particularly when the effect of high strain rates or strain softening is taken into account. Abrupt changes between old and new mesh lead to difficulty in transferring history-dependent variables accurately from one mesh to another. For such situations, it is better to control element sizes throughout the analysis domain by using a mesh density function, with fine elements inside the deformation mechanism and a coarse mesh elsewhere. The approximate extent of the deformation mechanism is easy to estimate for most geotechnical problems due to the simple geometry of the structural elements. Furthermore, for those problems free from soil surface effects, such as deep penetration of a cylindrical T-bar or a spherical ball (Figure 1), the remeshing stage

can be simplified by merely translating the initial mesh downward with the penetrometer, maintaining a fixed mesh relative to the penetrometer (Zhou and Randolph, 2007). This results in an essentially Eulerian method of analysis, but where the advection of history parameters is accomplished by interpolation.

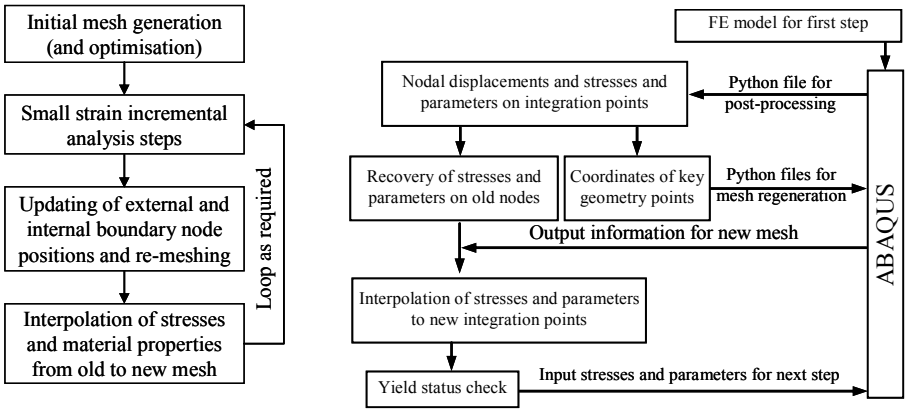

(a) Overall scheme (b) Implementation in ABAQUS

Figure 2. Overview of RITSS approach (Hu and Randolph, 1998a)

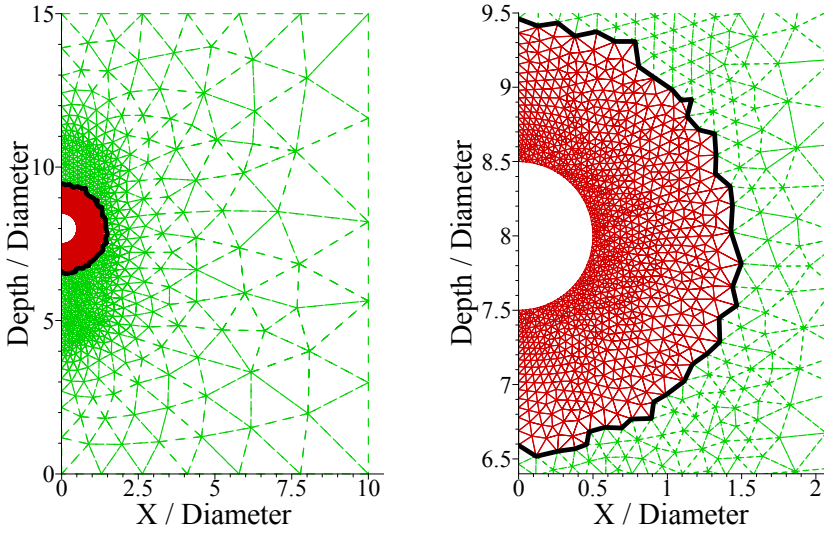

(a) Entire mesh (b) Close-up

Figure 3. FE mesh of T-bar and partial remeshing technique (Zhou et al. 2008)

An important advance in mesh regeneration for LDFE analysis was the partial remeshing technique developed by Barbosa-Cruz (2007), and further improved by Zhou et al. (2008). As discussed later, transferring of values from the old to the new Gauss points inevitably induces some degree of numerical diffusion, regardless of how accurate the interpolation algorithm is, unless the old and new Guass poins are exactly in the same location. In an attempt to minimise the numerical diffusion, a partial remeshing technique is adopted, whereby only the part of the domain undergoing large strains is re-discretised in the remeshing step; in the remaining (small strain) region, the nodal coordinates are merely updated according to the displacements. This technique is illustrated in Figure 3, after a cyclindrical T-bar has been penetrated by 2.5 diameters. The area close to the T-bar, demarcated by a thick curved line, is remeshed, In the remote area, the mesh is only updated to eliminate interpolation. The much finer elements in the remeshing zone are to minimise numerical diffusion. It is worth noting that the transition from the fine elements around the T-bar to the coarse mesh in the remote demain should be gradual and smooth. A comparison of interpolation accuracy between translating the initial mesh with the penetrometer (left half of each figure) and the partial remeshing approach (right half of each figure) is illustrated later in Figure 7, which shows contour plots of shear strength, s_{us} (calculated based on accumulated plastic shear strain), normalised by the original strength, s_{u0}. It can be seen that the partial remeshing technique minimises the interpolation pollution effectively, reducing diffusion of the zone of reduced shear strength.

The accuracy of large deformation analyses based on RITSS depends largely on that of the interpolation technique employed to map history-dependent variables from old to new mesh. In AFENA based RITSS, the

initial approach was a modified form of the unique element method, where values at each Gauss point were obtained primarily by interpolating from the three Gauss points of the old element containing the new Gauss point, but with modifications where extrapolation was required (Hu and Randolph, 1998b). More recently, good results have been obtained by triangulating the old and new Gauss points and then interpolating field quantities linearly for each new Gauss point from the triangle of old Gauss points within which it falls. The few new boundary Gauss points that fall outside the mesh of old Gauss points are treated specially, assigning a value obtained by using a linear interpolation between the two old boundary Gauss points lying to either side of the new Gauss point (Zhou and Randolph, 2007). This appears to largely eliminate error accumulation along the boundary during repeated remeshing and interpolation.

In ABAQUS based analyses, the Superconvergent Patch Recovery (SPR) (Zienkiewiecz and Zhu, 1993) and Recovery by Equilibration of Patches (REP) (Boroomand and Zienkiewicz, 1997) are favoured over that employed in AFENA based analyses to increase efficiency for 3D problems. Comparing SPR and REP, SPR is more efficient but needs the existence of optimal sampling points which are suspect for tetrahedral elements, while REP is free from this restriction. Therefore REP is better for 3D analysis. The drawback of REP, however, is that it cannot be used in effective stress analyses since its approximation of force equilibrium is deduced from total stresses. When SPR or REP is used, the boundary nodes cannot act as patch assembly points, so each boundary node must be attached to at least one interior patch of elements for recovery.

Following interpolation, the yield status is checked for new Gauss points and the stresses are corrected back to the yield surface if they do not lie on the current yield surface (Potts and Gens, 1985). The correction is essential to obtain an accurate and smooth displacement-resistance response. This is relatively easy for simple elastic-perfectly plastic models, where only stresses and yield status are needed in the correction. For more advanced (and complex) constitutive models, such as the Modified Cam-Clay (MCC) model, the correction becomes much more complicated. In addition to the stresses and yield status of each Gauss point, more parameters are needed in the correction process, such as magnitudes of the current loading surface, yield locus and stress ratio (ratio of deviatoric stress to mean effective stress). Currently, extensive efforts are being made to implement the MCC model for coupled large deformation analyses, to investigate the effect of loading rate (or partial consolidation) on the penetration response of offshore foundations and penetrometers.

3 Shallow embedment of pipelines – comparison between AFENA and ABAQUS

The most challenging geotechnical design issues associated with offshore pipelines are lateral buckling and axial 'walking' due to thermal expansion and contraction during operation. Accurate estimation of the as-laid embedment is important in order to assess the soil resistance to axial and lateral motion of the pipeline (Bruton et al., 2007; White and Randolph, 2007). As the pipe is laid on the seabed it penetrates the soil under a combination of self-weight and transient loading due to the laying process, accompanied by soil heave to either side. This process is essentially a large deformation problem, associated with large strains and changing geometry, requiring an allowance for the effect of soil heave, which contributes to the penetration resistance.

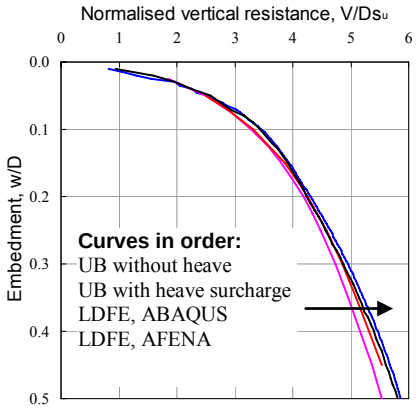

Figure 4. Resistance-embedment curves

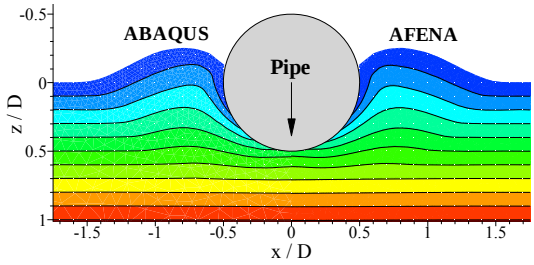

Figure 5. Deformation pattern at w/D = 0.45

Here, in addition to investigating the soil heave during pipe penetration from the surface, the performance of LDFE analyses based on ABAQUS and AFENA were compared. In both undrained simulations, a linear strength profile of $s_u = s_{um} + kz$ was modelled (with s_{um} being the undrained shear strength at the mudline, k the soil strength gradient and z the depth), with $kD/s_{um} = 1.25$ where D is the pipeline diameter. The elastic response was defined by a modulus ratio, $E/s_u = 500$, and Poisson's ratio of 0.499. The effective unit weight of the soil, γ', was taken such that $\gamma'D/s_{um} = 2.26$. Nodal joints were used along the pipe-soil interface, with a limiting shear stress taken as αs_{um}, with $\alpha = 0.31$. The resistance-embedment responses, with the vertical force, V, normalised by the pipeline diameter and local shear strength at the pipeline invert, are plotted in Figure 4 together with upper bound

plasticity solutions (Randolph and White, 2008). The difference in resistance between these two approaches is marginal; both are slightly larger than the upper bound solution with heave, where the heave is simplified as surcharge. Figure 5 compares the deformation pattern at an embedment of 0.45D and Figure 6 shows heave profiles at various ratios of w/D between 0.05 and 0.45. Both figures demonstrate clearly the excellent agreement between ABAQUS based and AFENA based LDFE approaches.

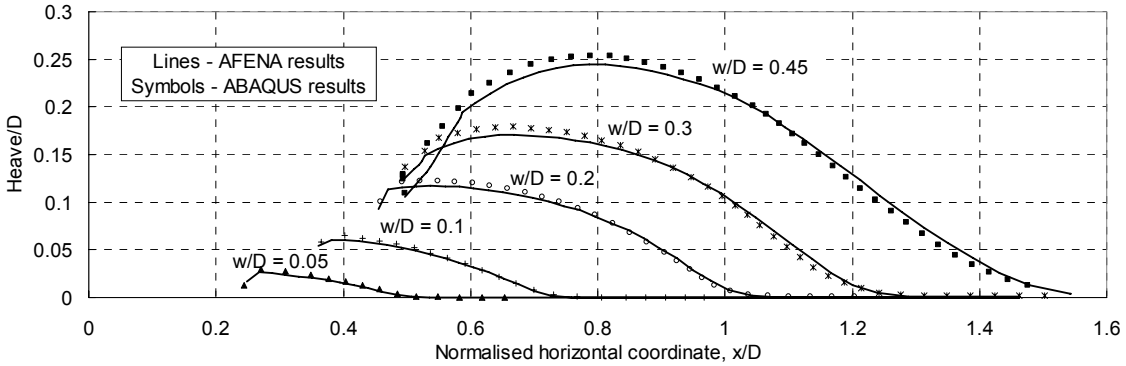

Figure 6. Heave profiles at different pipeline penetrations

4 Monotonic and cyclic penetration of cylindrical and spherical penetrometers – strain rate and strain softening effects

Cylindrical T-bar and spherical ball penetrometers are now widely used for offshore site characterisation in soft sediments as an alternative or supplement to conventional piezocone tests (Figure 1). During penetration, soil is able to flow around the penetrometer, instead of being forced outwards as with the cone penetrometer. Full-flow penetrometers offer several important advantages over the cone, such as improved resolution of the measured resistance, reduced uncertainty due to the overburden stress correction required for the cone penetrometer, and (for ideal perfectly plastic soil) the existence of closely-bracketed plasticity solutions for the resistance factor relating penetration resistance to the shear strength of the clay (Randolph, 2004). Both the intact and remoulded undrained shear strength can be deduced from the resistances measured during monotonic penetration and cyclic penetration and extraction tests .

To improve data interpretation from *in situ* T-bar or ball testing, the large deformation approach is necessary due to its particular capability in capturing relative flow of soil past the penetrometers.This is critical for modelling the evolving non-uniform distribution of shear strength due to strain-softening at different locations relative to the penetrometer. The linear elastic-perfectly plastic Tresca model was modified to allow for rate-dependency of shear strength and gradual strength degradation as the soil is sheared and remoulded (Zhou and Randolph, 2007). The undrained shear strength at individual Gauss points, s_u, is modified according to the current rate of maximum shear strain, $\dot{\gamma}_{max}$, and accumulated absolute plastic shear strain, ξ, expressed as

$$s_u = \left[1 + \mu \log\left(\frac{\max\left(|\dot{\gamma}_{max}|, \dot{\gamma}_{ref}\right)}{\dot{\gamma}_{ref}}\right)\right]\left(\delta_{rem} + (1-\delta_{rem})e^{-3\xi/\xi_{95}}\right)s_{u,ref} \quad (1)$$

The first bracketed term represents the enhancement due to high strain rates relative to a reference value, $\dot{\gamma}_{ref}$ (here taken as 1 %/hour, or 3 x 10^{-6} s^{-1}), following a logarithmic law with a rate parameter, μ. The second term models the degradation of strength according to an exponential function of accumulated plastic shear strain, ξ, from the intact condition to a fully remoulded state. δ_{rem} is the strength ratio of soil between fully remoulded and intact states (the inverse of the sensitivity, S_t). The relative ductility is controlled by the parameter, ξ_{95}, which represents the cumulative shear strain required for 95 % remoulding. Its magnitude may be deduced from laboratory test data, taking acount of any strain concentrations within shear bands, or by conducting cyclic penetration and extraction tests using full-flow penetrometers. Typical values are found to be around 10 to 50 (Einav and Randolph, 2005). $s_{u,ref}$ is the original shear strength at the reference shear strain rate prior to any softening. A more detailed discussion may be found in Zhou and Randolph (2007).

During the process of continuous penetration, periodic shear bands were observed for relatively brittle soil from the regions with most severely softened shear strength, s_{us} (Figure 7). They evolved cyclically ahead of the advancing cylindrical and spherical penetrometers, and resulted in oscillations in the resistance-penetration response. Similar shear bands were also observed in centrifuge tests of pipe penetrating in soft clay, using advanced image analysis technique based on Particle Image Velocimetry and photogrammetry (Dingle et al., 2008; Zhou et al., 2008). Further parametric study found that this phenomenon became increasingly pronounced with reducing strain-softening parameters, ξ_{95} and δ_{rem} (increasing the relative brittleness of the soil), but tended to be suppressed by increasing the strain-rate dependency of shear strength (Zhou and Randolph, 2007). The effect of rate dependency on resistance response is illustrated in Figure 8. Initially, the T-bar was wished in place

at 5.5 diameters below the soil surface before being advanced by 2.5 diameters to establish a steady state, with a rate parameter, μ of 0.1, strain-softening parameter, ξ_{95} of 15 and δ_{rem} of 0.2 (i.e. S_t = 5). Then the rate parameter was reduced gradually to 0.05 over a penetration of 0.5 diameter, followed by further penetration of 2 diameters. By comparing with the response with a constant rate parameter, μ of 0.05 in Figure 8, it is clear that the oscillations in resistance-penetration response can be suppressed by high rate dependency.

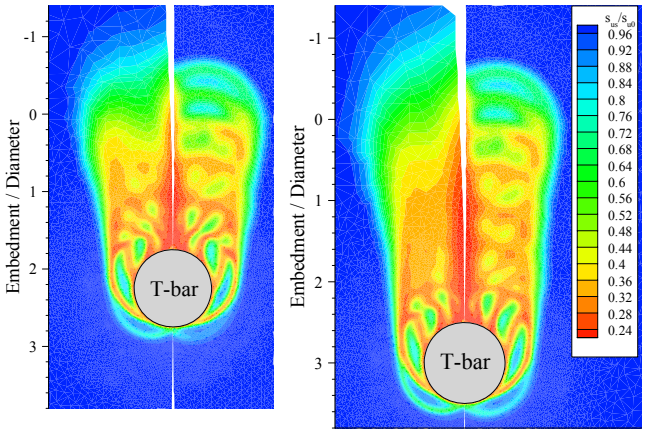

(a) Penetration = 2.25D (b) Penetration = 3D

Figure 7. Periodic shear bands and interpolation accuracy without (left half) and with (right half) partial remeshing

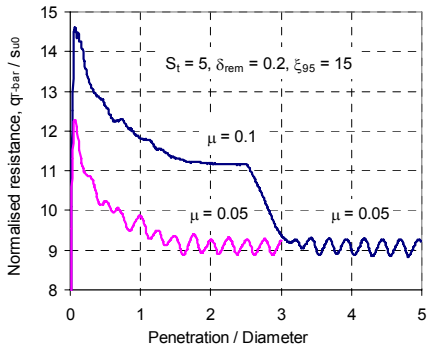

Figure 8. Resistance-penetration response under varying strain-rate dependency

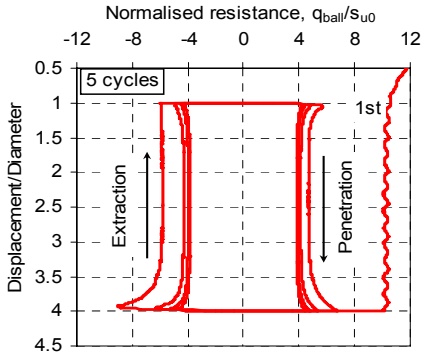

Figure 9. Typical cyclic response for the Ball

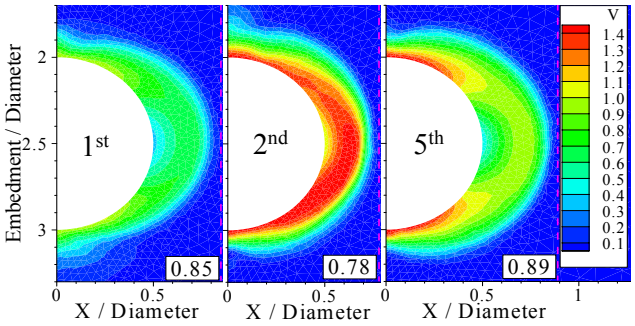

Figure 10. Evolution of mechanism widths

An important advantage of full-flow penetrometers is their potential to evaluate the remoulded shear strength *in situ*, by repeated motion of penetration and extraction within a narrow depth range in order to remould the soil locally within a rectangular slot (T-bar) or cylindrical column (ball). Figure 9 shows a typical cyclic resistance-penetration (extraction) response for the ball with μ = 0.05, ξ_{95} = 10 and S_t = 5. There is a marked decrease in resistance for the second penetration relative to the first, reflecting remoulding of the surrouding soil. The resistance becomes stable after the fourth penetration. Corresponding evolution of mechanism widths are shown in Figure 10 for the first, second, and fifth (last) penetration strokes, in the format of contours of incremental displacements normalised by the specified displacement increment in the middle of the cyclic penetration zone. Interestingly, the failure mechanism reduces dramatically during early cycles as a result of rapid softening of the material close to the penetrometer. In later cycles, however, material further away from the penetrometer continues to soften, and the mechanism grows in size towards the optimum appropriate for a fully rough penetrometer (since the interface friction is assumed equivalent to the remoulded shear strength in the present analyses). Detailed description of large deformation finite element analysis simulating cyclic penetration and extraction of full-flow penetrometers is provided in Zhou et al. (2008).

5 Penetration of spudcan foundations for mobile drilling rigs – soil strength and layer effect

Most offshore drilling in shallow to moderate water depths is performed from self-elevating (jack-up) mobile drilling units with proven operational versatility and mobility, and now capable of operating in water depths up to 130 m. A typical modern jack-up unit comprises a buoyant triangular platform rested on vertically retractable three independent truss-worked legs, and a large inverted conical footing, known as a 'spudcan', is used widely to support each leg (Young et al., 1984). Spudcans are effectively circular or polygonal in plan, with a shallow conical underside and a central spigot to provide improved sliding resistance.

Prior to commencing jack-up rig operations, spudcans are proof loaded by static vertical preloading to obtain an acceptable margin of safety against the extreme storm design event within the capacity envelope (SNAME, 2002). Spudcan foundations undergo progressive penetration, with final penetration more than two diameters in clay strata, during preloading, unlike onshore pre-embedded foundations or offshore skirted foundations. This continuous penetration involves changing of soil flow directions with penetration depth and large distortion and significant remoulding of the soil (Hossain et al., 2005, 2006, 2007). However, spudcan penetration is generally assessed by considering the bearing capacity profile obtained form a series of 'wished in place' spudcans at successively increasing depths. The bearing capacity factors originally developed for a surface footing (Skempton, 1951; Brown and Meyerhof, 1969) are adjusted for embedment depth and soil strength heterogeneity. Alternative factors of Martin (2001) and Houlsby and Martin (2003) are for a cone with cylindrical side walls, embedded in soil with strength increasing linearly with depth, but transversely isotropic. These approaches involve significant idealisation, with no account taken of the changes in flow regime of the soil or the complex evolving pattern of soil strengths in the vicinity of the spudcan during progressive penetration.

Simulation of spudcan penetration during preloading requires continuous penetration analysis. LDFE analyses were undertaken by pushing spudcan foundations continuously from the soil surface in non-homogeneous clay with strength increasing with depth and layered clay deposits comprising a stiff layer underlain by a soft layer. The analyses were also conducted without and with taking strain-softening and rate dependency into account. Initially, soil beneath the spudcan is displaced outwards and upwards towards the soil surface, leading to heave at the mudline and the formation of a cavity above the spudcan, as depicted in the bottom-left corner of Figure 11a. With further penetration, soil starts to flow around the spudcan, back into the cavity, and eventually provides a seal on the spudcan top, limiting the cavity depth (see the bottom-left corner of Figure 11b).

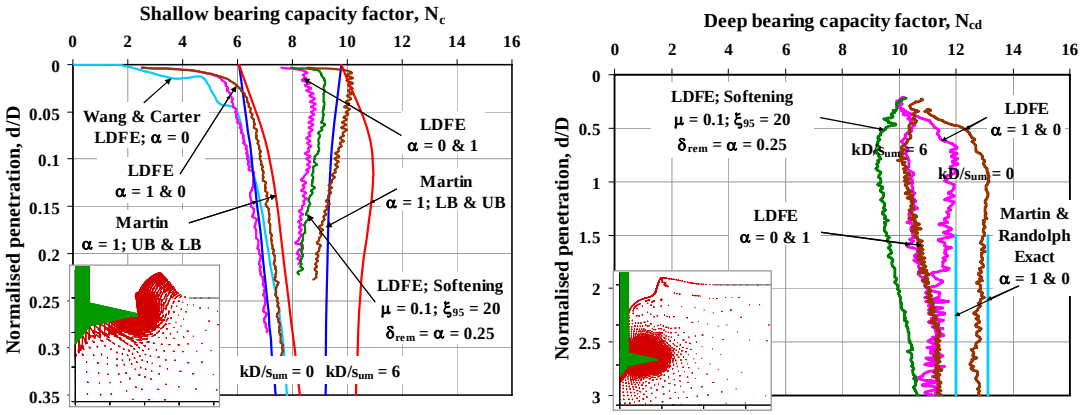

(a) Shallow bearing capacity factor (b) Deep bearing capacity factor

Figure 11. Bearing capacity factors for spudcan in non-homogeneous clay

Figure 11 also illustrates the load-penetration responses for smooth and rough-based spudcans in non-homogeneous clays with non-homogeneity factor $kD/s_{umi} = 0$ ($s_{umi}/\gamma' D = 0.095$, where the suffix i stands for intact and D is the spudcan diameter) and $kD/s_{umi} = 6$ ($k/\gamma' = 0.29$). The results are presented in terms of a shallow bearing capacity factor, N_c, prior to any back-flow, calculated by considering the penetration resistance (relative to the buoyant weight of the spudcan) as

$$q_u = N_c s_{u0i} + \gamma' d + \gamma' \frac{V}{A} \tag{2}$$

and a deep bearing capacity factor, N_{cd}, after initiation of back-flow, by considering the penetration resistance as

$$q_u = N_{cd} s_{u0i} + \gamma' \frac{V}{A} \tag{3}$$

where V is the embedded volume of the spudcan and shaft and s_{u0i} the intact shear strength at the level of the spudcan maximum diameter. Other numerical and plasticity solutions are included in Figure 11 for comparison.

For shallow penetration (Figure 11a), spudcan base roughness and the degree of soil strength non-homogeneity are found to have significant influence on the bearing capacity, which increases with increasing α and kD/s_{umi}. Accounting for strain-softening and rate dependency with typical parameters ($\xi_{95} = 20$, $\mu = 0.1$, $\dot{\gamma}_{ref} = 3 \times 10^{-6}$/s, $\delta_{rem} = 0.25$), the factors for $\alpha = 0.25$ do not exhibit any substantial influence other than sharp rising at the beginning. The LDFE analysis for a flat circular footing from Wang and Carter (2002) and plasticity solutions from Martin (2001), both for cylindrical geometries in weightless soil, can be compared with the situation of a spudcan with a cavity above it. For a smooth base, the curve from this study lies marginally below the one of Wang and Carter. For a rough base, LDFE results are nicely bracketed by the bound solutions of Martin (2001).

For embedded foundations on an ideally elastic-perfectly plastic soil, the effect of strength non-homogeneity should exist only at shallow depths, before the transition to a localised flow-round mechanism. Once penetration is sufficient for the full flow-round mechanism to govern, the limiting value should become independent of kD/s_{umi}, depending only on the spudcan roughness. Indeed, Figure 11b largely reflects this, except for the rough spudcan on clay with $kD/s_{umi} = 6$, where there appears to be little effect of α. This is largely owing to the effects of soft soil being carried down with the spudcan. The distortion of the soil layers by the advancing spudcan is depicted for this case in Figure 12, plotting strength contours for the soil after a penetration of 1 diameter. The spudcan is surrounded by softer material, within which the flow mechanism occurs and where the shear strength will be less than the nominal value (s_{u0i}) at that penetration (Equation 3). Nevertheless, the ultimate limiting N_{cd} value of about 11.4 for a smooth spudcan, and in non-homogeneous clay regardless of roughness, is slightly lower than the exact value for a smooth thin plate (Martin and Randolph, 2001), owing to the sloping top and bottom surfaces of the spudcan. For a rough spudcan on uniform clay ($kD/s_{umi} = 0$), the limiting value of N_{cd} is about 12.8, which agrees reasonably well with the exact value of 13.11 (Martin and Randolph, 2001), and is nicely bracketed by the bound solutions for an embedded circular footing, where lower and upper bound values of N_{cd} are 11 and 13.7 (Salgado et al., 2004).

As a final observation, spudcan penetration in more realistic soil conditions, with typical strain-softening and rate dependency, shows a significant reduction in penetration resistance, with bearing capacity factors that are about 10 % lower value over the full range of penetration (Figure 11b).

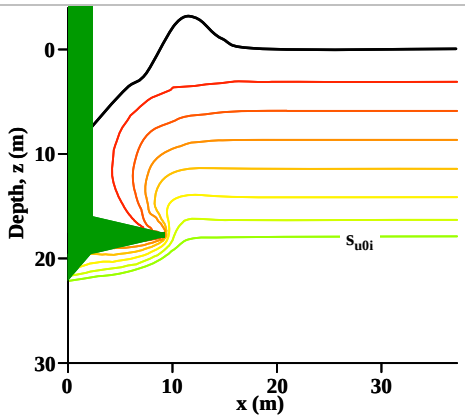

Figure 12. Strength contour of a rough-based spudcan penetration (d/D = 1; $kD/s_{umi} = 6$)

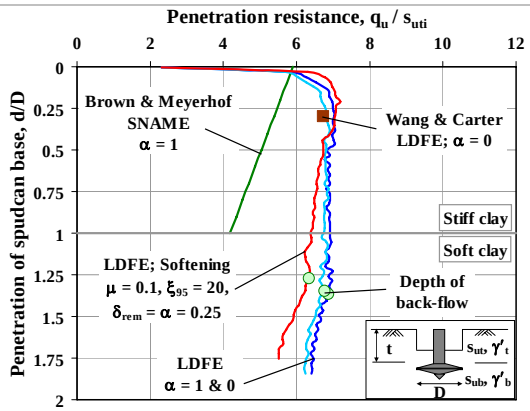

Figure 13. Bearing capacity for spudcan in layered clay ($s_{ubi}/s_{uti} = 0.4$; $s_{uti}/\gamma_t'D = 0.78$; t/D = 1)

Jack-up preloading in stratified deposits, where a strong layer overlays weaker soil, has always been a challenging case with the potential for catastrophic 'punch-through' failure. Such incidents continue to occur at an alarming rate all over the world. Sudden large uncontrolled penetration, usually experienced by only one leg, may lead to buckling of the leg, effectively decommissioning the platform, or may even result in toppling of the unit (Young et al., 1984; Brennan et al., 2006). LDFE analysis has been carried out on spudcan penetration in two layer (stiff-over-soft) clay in order to explore this phenomenon. The parameters varied include the intact strength ratio between lower and upper soil layers (s_{ubi}/s_{uti}), the thickness of the upper layer relative to the spudcan diameter (t/D) and the normalised strength and its gradient of the lower layer. Once again analyses were performed without (for $\alpha = 0$ and 1) and with (for $\mu = 0.1$; $\xi_{95} = 20$; $\delta_{rem} = \alpha = 0.25$) taking strain softening and rate dependency into account. Figure 13 plots penetration responses for a typical case with $s_{ubi}/s_{uti} = 0.4$, $s_{uti}/\gamma_t'D = 0.78$ and t/D = 1, with the penetration resistance normalised by the intact shear strength of the upper layer, s_{uti}, after allowing for the buoyancy effect of the spudcan (as in Equation 3).

In contrast to the situation in clay with linearly increasing strength, a plug of stiff material from the upper layer is trapped beneath the spudcan and is pushed down with the advancing spudcan into the lower layer. Consequently, the effect of spudcan base roughness is found to be minimal. A peak in penetration resistance, followed by a reduction, resulting in a potential punch-through situation, is exhibited by all cases, but is most pronounced where strain-softening is taken into account. Current offshore design guidelines for assessing spudcan penetration response (SNAME, 2002) recommend a bearing capacity factor calculated following Brown and Meyerhof (1969), but adjusted for embedment depth by applying a constant depth factor, following the semi-empirical approach of Skempton (1951). However, Brown and Meyerhof conducted model tests on a surface footing with very small displacement prior to failure, and under 1 g conditions without maintaining stress similitude in terms of $s_u/\gamma'D$. Thus their approach does not account for the distortion of the upper layer as it punches through into the lower layer, and indeed provides an unduly conservative estimate of penetration resistance. Progressive embedment in layered soils is affected by a number of interacting features, as discussed by Wang and Carter (2002), who carried out LDFE analyses for weightless soil ($\gamma' = 0$) for a circular (cylindrical) footing with smooth base. In all LDFE analyses of spudcan penetration shown here, the open cavity depth exceeded the thickness of

the upper soil layer, mimicking the situation for a cylindrical footing. Wang and Carter's curve therefore shows a similar trend and closely matching peak bearing resistance.

6 Uplift capacity of circular and square anchors – 3D analysis

Plate anchors are being used increasingly to moor large floating structures in deep or ultra-deep water. They are generally installed vertically using a mandrel or suction caisson, and then rotated (or 'keyed') until they are aligned perpendicular to the mooring cable. Plate anchors are usually rectangular in shape, with typical aspect ratios less than 2, rather than a circular or strip geometry, hence the need for 3D simulations. As observed in model tests (Das, 1980; Das and Singh, 1994) and early FE studies (Rowe and Davis, 1982), plate anchors may undergo large displacement before reaching their ultimate uplift capacity. Furthermore, the soil beneath the anchor base always moves with the anchor initially, before gradual separation occurs. It is difficult for small scale (1 g) model tests, plasticity limit solutions or small strain FE analysis to simulate the continuous pulling-out process. Hence an LDFE approach has been followed to explore the behaviour of plate anchors for two simplified cases, namely 'no breakaway' (where no separation is permitted between the anchor base and soil) and 'immediate breakaway' (where the soil is free to separate from the anchor base once the loading is applied). Compared with the alternative methods mentioned above, the 3D RITSS approach can simulate both the simplified cases and continuous pulling-out process, to investigate the effect of overburden pressure, soil stiffness and anchor aspect ratio on the uplift capacity (Wang et al., 2007).

For anchors buried deeply but with immediate breakaway allowed, the ultimate capacity is usually accompanied by a significant displacement, typically greater than 1B, where B is the anchor width. Even where small strain FE calculations can achieve convergence, the accuracy of results for such large displacements is suspect due to severe mesh distortion in the vicinity of the anchor. In fact, in early studies of strip anchors, Rowe and Davis (1982) proposed a 'cut-off'' criterion, with the ultimate capacity defined in terms of a limiting displacement. Merifield et al. (2003) provided finite-element based plasticity limit solutions for rectangular and circular anchors, with the soil response treated as rigid-perfectly plastic. In Figure 14, the computed ultimate capacity factors, N_{co}, for different embedment ratios, H/B, in uniform weightless soil and fully rough (upper) interface between anchor and soil, are compared with data from 1 g model tests (Das and Singh, 1994) and lower bound solutions for weightless soil (Merifield et al., 2003). Overall, the LDFE results agree well with the test data, but lie up to 13 % below the lower bound solutions for deeply embedded anchors. This is due to the rigid-plastic assumption in the lower bound solutions, with infinite modulus ratio, E/s_u. For the LDFE results in Figure 14, the normalised Young's modulus of the clay was selected as $E/s_u = 500$. When E/s_u was increased to 1000 and 2000, as shown in Figure 15, the ultimate capacity increased and became closer to the lower bound solutions for deep anchors. The capacity factor with $E/s_u = 2000$ was just above the lower bound solution for H/B = 5, and just below it for H/B = 6. Capacity factors from small strain FE analysis were available for $H/B \leq 5$, and were always higher than both the lower bound solutions and LDFE results. The reason is that small strain calculations are based on the original mesh, which is in accordance with the assumption of limit analyses that the soil does not deform before the onset of plasticity. However, in practice, full mobilisation of the capacity requires finite anchor displacement, with the magnitude depending on the soil stiffness, so that the soil stiffness affects the failure mechanism during continuous pullout with breakaway allowed.

The anchor capacity factor obtained for weightless soil may be adjusted to allow for overburden pressure by simple superposition according to

$$N_{c\gamma} = N_{c0} + \frac{\gamma H}{s_u} \leq N_{cu} \tag{4}$$

where N_{co} is the breakaway factor for weightless soil. The first part of this expression implies that the capacity will increase without limit with increasing embedment of anchor. However, as noted by Merifield et al. (2003), and confirmed through LDFE analyses (Wang et al., 2007), a limiting capacity factor (N_{cu}) is eventually achieved, independent of overburden pressure, once the anchor is embedded sufficiently deeply. At that stage, the failure mechanism is localised in the vicinity of anchor and the limiting capacity factor corresponds to that for the no breakaway condition. The exact capacity factor of 13.11 proposed by Martin and Randolph (2001) is for the deep (circular) anchor case. An example set of LDFE results is shown in Figure 15 for $s_u/\gamma'B = 0.14$, where γ' is the effective unit weight of soil (assuming offshore conditions with free water present at the soil surface). The capacity factor becomes constant, with $N_{cu} = 13.8$, once the embedment is deeper than 1.2B. The difference of 5 % compared with the exact solution (for circular anchor) is partly due to the finite thickness of the anchor in the LDFE analyses, where the thickness ratio was t/B = 0.025.

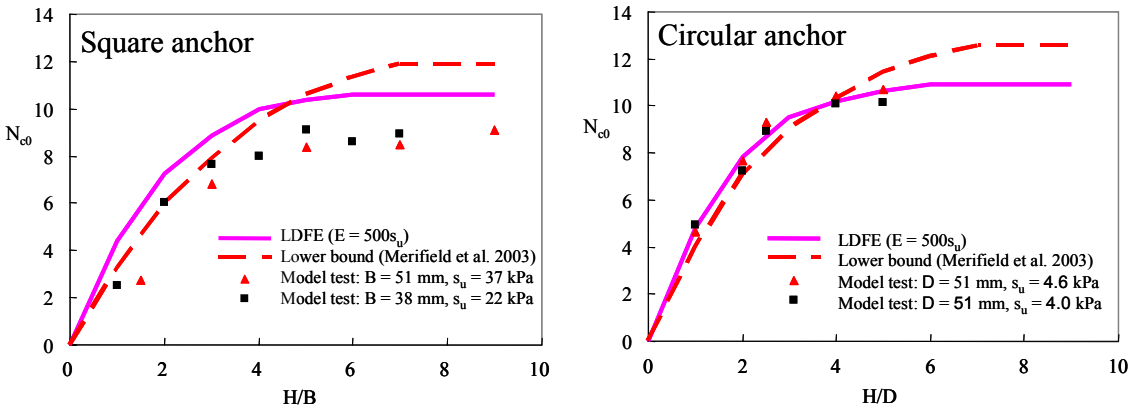

Figure 14. Breakout factors for square and circular anchors in weightless soil

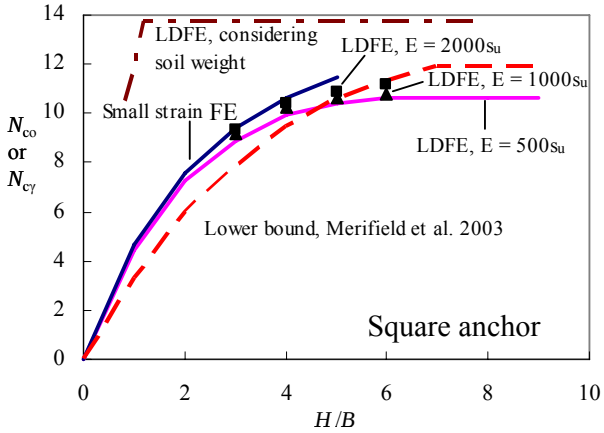

Figure 15. Effect of Young's modulus and soil weight on breakout factor

7 Conclusions

A simple and powerful approach – Remeshing and Interpolation Technique with Small Strain model (RITSS) - has been applied to a variety of offshore foundation and anchoring problems, including surface penetration of pipelines, deep penetrometer response, surface penetration of spudcan foundations and breakout capacity of plate anchors. Large deformation finite element (LDFE) results based on RITSS in conjunction with AFENA and ABAQUS have been compared between each other, using plasticity solutions for benchmarks; the effects of strain softening, strain rate and non-homogeneous soil strength, including soil layering, have been investigated; and the technique has also been applied to 3D geometries. The following conclusions can be drawn.

The advantage of the RITSS approach is that, by using a small strain formulation for the incremental solution steps, it can be implemented easily in any existing finite element package even for relatively complex soil models. This has been demonstrated for pipeline analysis, where the LDFE results from AFENA and ABAQUS were essentially identical and also close to upper bound solutions. The soil heave to either side of the pipe during penetration gave only a small increase in resistance, but is important for lateral breakout calculations.

Analysis of full-flow penetrometers in strain-softening and rate dependent soil has been accomplished by simple updating of the soil shear strength at each remeshing stage. Partial remeshing was shown to be effective in limiting numerical diffusion of the remoulded zone. Oscillation in the penetration resistance occurred due to the periodic generation and softening of shear bands, being more pronounced in brittle soil, and gradually suppressed with increasing strain rate dependency of soil strength.

LDFE analysis of spudcan penetration in clay with strength increasing linearly with depth, and in layered clay, has allowed identification of different modes of failure and corresponding alternative expressions for calculating the penetration resistance. A limiting bearing capacity factor was reached at deep penetration and compared well with plasticity solutions for flat-based circular foundations. Punch-through failure in layered soil was found to be more pronounced for soil with strain softening characteristics.

The LDFE has been successfully extended to 3D analysis for plate anchors, where it was shown that anchor capacities may fall below lower bound plasticity solutions because of pre-failure (elastic) deformations. The anchor capacity was shown to increase with increasing E/s_u ratio, approaching the rigid-plastic solutions. Overall the LDFE approach explored in this paper has the potential to be applied to any foundation analysis, even for relatively complex soil models or where 3D analysis is required.

8 References

Barbosa-Cruz, E.R. 2007. *Partial consolidation and breakthrough of shallow foundations in soft soil*. Ph.D. Thesis, The University of Western Australia, Perth, WA, Australia.

Bathe, K.J., Ramm, E., Wilson, E.L. 1975. Finite element formulations for large deformation dynamic analysis. *Int. J. Numer. Methods Eng.*, 9, 353-386.

Boroomand, B., Zienkiewicz, O.C. 1997. An improved REP recovery and the effectivity robustness test. *Int. J. Numer. Methods Eng.,* 40, 3247-3277.

Brennan, R., Diana, H., Stonor, R.W. P., Hoyle, M.J.R., Cheng, C.-P., Martin, D., Roper, R. 2006. Installing jackups in punch-through-sensitive clays. *Proc. Offshore Technology Conference*, Houston, OTC 18268.

Brown, J.D., Meyerhof, G.G. 1969. Experimental study of bearing capacity in layered clays. *Proc. 7th Int. Conf. on Soil Mech. and Found. Engng.*, Mexico, 2, 45-51.

Bruton D., Carr M., White D.J. 2007. The influence of pipe-soil interaction on lateral buckling and walking of pipelines: the SAFEBUCK JIP. *Proc. 6th Int. Conf. on Offshore Site Investigation and Geotechnics,* London, UK.

Carter, J.P., Balaam, N.P. 1995. *AFENA User Manual 5.0*. Geotechnical Research Centre, The University of Sydney, Sydney, Australia.

Das, B.M. 1980. A procedure for estimation of ultimate capacity of foundation in clay. *Soils and Foundations*. 20(1), 77-82.

Das, B.M., Singh, G. 1994. Uplift capacity of plate anchors in clay. *Proc. 4th Int. Offshore and Polar Engineering Conf.*, Osaka, Japan, 436-442.

Dingle, H.R.C., White, D.J., Gaudin, C. 2008. Mechanisms of pipe embedment and lateral breakout on soft clay. *Accepted for publication in Canadian Geotechnical Journal.*

Einav, I., Randolph, M.F. 2005. Combining upper bound and strain path methods for evaluating penetration resistance. *Int. J. Numer. Meth. Engng.*, 63, 1991-2016.

Ghosh, S., Kikuchi, N. 1991. An arbitrary Lagrangian-Eulerian finite element method for large deformation analysis of elastic-viscoplastic solid. *Comput. Methods Appl. Mech. Eng.*, 86(2), 127-188.

Hossain, M.S., Hu, Y., Randolph, M.F., White, D.J. 2005. Limiting cavity depth for spudcan foundations penetrating clay. *Géotechnique*, 55(9), 679-690.

Hossain, M.S., Randolph, M.F., Hu, Y. White, D.J. 2006. Cavity stability and bearing capacity of spudcan foundations on clay. *Proc. Offshore Technology Conference*, Houston, OTC 17770.

Hossain, M.S., Randolph, M.F. 2007. Investigating potential for punch-through for spudcan foundations on layered clays. *Proc. 17th Int. Offshore and Polar Engineering Conf.*, Lisbon, 2, 1510-1517.

Houlsby, G.T., Martin, C.M. 2003. Undrained bearing capacity factors for conical footings on clay. *Géotechnique*, 53(5), 513-520.

Hu, Y., Randolph M.F. 1998a. A practical numerical approach for large deformation problems in soil. *Int. J. Num. and Anal. Methods in Geomech.*, 22(5), 327-350.

Hu, Y., Randolph M.F. 1998b. H-adaptive FE analysis of elasto-plastic non-homogeneous soil with large deformation. *Computers and Geotechnics*, 23(1), 61-83.

Hu, Y., Randolph, M.F., Watson, P.G. 1999. Bearing response of skirted foundations on non-homogeneous soil, *J. Geotech. Engrg.*, ASCE, 125(12), 924-935.

Hughes, T J.R., Winget, J. 1980. Finite rotation effects in numerical integration of rate constitutive equations arising in large-deformation analysis. *Int. J. Numer. Meth. Engng.*, 15, 1862-1867.

Konuk, I., Yu, S. 2007. Continuum FE modeling of lateral buckling: study of soil effects. *Proc. 26th Int. Conf. on Offshore Mechanics and Arctic* Engng*., OMAE07*, San Diego, Paper OMAE2007-29376.

Liu, W.K., Belytschko, T., Chang, H. 1986. An arbitrary Lagrangian–Eulerian finite element method for path-dependant materials. *Comput. Methods Appl. Mech. Eng.*, 58, 227-245.

Liu, W.K., Chang, H., Chen, J.S., Belytschko, T. 1998. Arbitrary Lagrangian–Eulerian Petrov–Galerkin finite elements for nonlinear continua. *Comput. Methods Appl. Mech. Eng.*, 68,259-310.

Liyanapathirana, D.S. 2008. Numerical simulation of T-bar penetration in soft clay. *Proc. GeoCongress 2008*, New Orleans.

Lu, Q., Hu, Y., Randolph, M.F. 2000. FE analysis for T-bar and spherical penetrometers in cohesive soil. *Proc. 10th Int. Conf. On Offshore and Polar Engng., ISOPE'00*, Seattle, 2, 617-623.

Martin, C.M. 2001. Vertical bearing capacity of skirted circular foundations on Tresca soil. *Proc. 15th Int. Conf. on Soil Mechanics and Geotechnical Engineering*, Istanbul, 1, 743-746.

Martin, C.M., Randolph M.F. 2001. Applications of the lower and upper bound theorems of plasticity to collapse of circular foundations. *Proc. 10th IACMAG*, Tucson, 2, 1417-1428.

Merifield, R. S., Lyamin, A.V., Sloan, S.W., Yu, H.S. 2003. Three-dimensional lower bound solutions for stability of plate anchor in clay. *J. Geotech. Geoenviron. Eng.*, 129(3), 243-253.

Nazem, M., Sheng, D., Carter, J.P. 2006. Stress integration and mesh refinement for large deformations in geomechanics. *Int. J. Numer. Methods Eng*., 65(7), 1002-1027.

Potts, D.M., Gens, A. 1985. A critical assessment of methods of correcting for drift from the yield surface in elasto-plastic finite element analysis. *Int. J. Numer. Anal. Meth. Geomech.*, 9(2), 149-159.

Randolph, M.F. 2004 Characterisation of soft sediments for offshore applications. *Proc. 2nd Int. Conf. on Site Characterisation*, Porto, Portugal,1, 209-231.

Randolph, M F., White, D.J. 2008. Upper bound yield envelopes for pipeline at shallow embedment in clay. *Accepted for publication in Géotechnique*.

Rowe, R.K., Davis, E.H. 1982. The behaviour of anchor plates in clay. *Géotechnique*, 32(1), 9-23.

Salgado, R., Lyamin, A.V., Sloan, S.W., Yu, H.S. 2004. Two- and three-dimensional bearing capacity of foundations in clay. *Géotechnique*, 54(5), 297-306.

Skempton, A.W. 1951. The bearing capacity of clays. *Building Research Congress*, London, 1, 180-189.

SNAME 2002. *Site specific assessment of mobile jack-up units. 1st Edition – Rev. 2*, Society of Naval Architects and Marine Engineers, New Jersey.

van Haaren, M.J., Stoker, H.C., van den Boogaard, A.H., Huétink, J. 2000. The ALE-method with triangular elements: direct convection of integration point values. *Int. J. Numer. Methods Eng*., 49, 697-720.

Wang, C.X., Carter, J.P. 2002. Deep penetration of strip and circular footings into layered clays. *Int. J. Geomech.*, ASCE, 2(2), 205-232.

Wang, D., Hu, Y., Jin, X. 2006. Two-dimensional large deformation finite element analysis for the pulling-up of plate anchor. *China Ocean Engineering*, 20(2), 269-279.

Wang, D., Hu, Y., Song, Z. 2007. Large deformation analysis of rectangular plate anchors in normally consolidated clay. *Proc. 10th Australia and New Zealand Conference on Geomechanics*, Brisbane, 268-273.

White, D.J., Randolph, M.F. 2007. Seabed characterisation and models for pipeline-soil interaction. Int. J. of Offshore and Polar Engineering, 17(3), 193-204.

Young, A.G., Remmes, B.D., Meyer, B.J. 1984. Foundation performance of offshore jack-up drilling rigs. *J. Geotech. Engrg.*, ASCE, 110(7), 841-859.

Zhou, H., Randolph, M.F. 2007. Computational techniques and shear band development for cylindrical and spherical penetrometers in strain-softening clay. *Int. J. Geomech.*, ASCE, 7(4), 287-295.

Zhou, H., Randolph, M.F., Andersen K.H. 2008. Numerical investigations into cycling of full-flow penetrometers in soft clay. *Submitted for publication.*

Zienkiewiecz O.C., Zhu J.Z. 1993. The superconvergent patch recovery and a posteriori error estimates. Part 1: The recovery technique. *Int. J. Numer. Methods Eng*., 33, 1331-1364.